

Sodium Thiosulfate-Coated Ceramic Denuders for Ozone Removal in Ultrafine Particle Sampling

5 Elisabeth Eckenberger¹, Andreas Mittereder², Nadine Gawlitta^{3,4}, Martin Sklorz^{3,4}, Dieter Brüggemann²,
Ralf Zimmermann^{3,4}, Anke C. Nölscher^{1*}

¹ Bayreuth Center of Ecology and Environmental Research (BayCEER), University of Bayreuth, Germany

² Department of Engineering Thermodynamics and Transport Processes, University of Bayreuth, Bayreuth, Germany

³ Joint Mass Spectrometry Centre (JMSC) at Comprehensive Molecular Analytics, Helmholtz Zentrum München, Neuherberg,
10 Germany

⁴ JMSC at Chair of Analytical Chemistry, Institute of Chemistry, University of Rostock, Rostock, Germany

* now at: Institute of Climate and Energy Systems - Troposphere (ICE-3), Forschungszentrum Jülich GmbH, Jülich, Germany,
and Institute of Geophysics and Meteorology, University of Cologne, Cologne, Germany

Correspondence to: Elisabeth Eckenberger (Elisabeth.eckenberger@uni-bayreuth.de), Anke C. Nölscher (a.noelscher@fz-
15 juelich.de)

Abstract. Ozone (O₃) remaining in sampling air can artefactually alter the chemical composition of collected ultrafine particles (UFP), biasing quantitative analysis of the chemical composition. In this study, we developed and evaluated a sodium-thiosulfate O₃ denuder (TSOD) specifically tailored for UFP sampling and assessed its O₃ scrubbing efficiency, particle losses, and chemical selectivity. In laboratory tests under controlled relative humidity and inlet O₃ levels up to 200 ppbV, the outlet concentration remained consistently ~~below between the instrumental detection limit 0 and 0.3 ppbV~~, demonstrating the O₃ removal efficiency of the TSOD. During an urban field deployment over 7 days O₃ downstream of the TSOD consistently remained ~~below the detection limit 0 ppbV~~ while ambient O₃ varied between 0 and 65 ppbV. Moreover, for particles with mobility diameters ranging from 10 to 1000 nm, we did not observe any significant losses in particle number concentrations. Using a parallel two-channel UFP sampler (with vs. without upstream TSOD), we quantified O₃-driven sampling artefacts in UFP mass focussing on three types of organic markers. (1) Firstly, we targeted polycyclic aromatic hydrocarbons (PAHs), particularly chrysene (Chry), benz[a]anthracene (BaA), benzo[a]pyrene (BaP), indeno[1,2,3-cd]pyrene (IcdP), benzo[k]fluoranthene (BkF), and benzo[b]fluoranthene (BbF). Without upstream O₃ removal, the individual concentration of the PAHs were 15 ± 2.9 – 46 ± 5.5 % lower. (2) Secondly, for the tire and road wear marker, the antioxidant N-(1,3-dimethylbutyl)-N'-phenyl-p-phenylenediamine (6PPD) and its oxidation product 6PPD-quinone (6PPDq), we observed in-situ ozonation of 6PPD to 6PPDq with transformation yields of about 13 ± 4.0 to 20 ± 8.3 %. (3) In contrast, biogenic organic acids (BOAs) did not show differences when sampled with or without O₃, as their O₃ reactivity is much lower than the one of the PAHs. Moreover, this test indicated that the TSOD did not perturb the gas-particle partitioning of these semi-volatile species.

Our results demonstrate that the TSOD (i) efficiently scrubs atmospheric O₃ at relevant mixing ratios, (ii) does not introduce measurable particle losses across 10–1000 nm, and (iii) preserves semi-volatile partitioning.

1 Introduction

Tropospheric ozone (O₃) is ubiquitous and highly reactive. Close to the Earth's surface, O₃ typically exhibits mixing ratios of up to 80 ppbV, occasionally exceeding 90 ppbV during strong photochemical episodes (Gaudel et al., 2018; Monks et al., 2015). Its tropospheric lifetime is on the order of days to weeks, typically 6–27 days depending on altitude and chemical environment (Prather & Zhu, 2024; Young et al., 2013). O₃ can damage leaf tissues, irritate eyes, and harm the respiratory system, making it an air pollutant with short and long-term effects on ecosystems and human health (Emberson, 2020; Zhang et al., 2019). In the atmosphere, O₃ reacts with a wide range of atmospheric organic compounds. While being an important oxidant and initiating the oxidative removal of unsaturated organic gaseous molecules, O₃ poses a challenge in sampling when these O₃-reactive molecules are targeted in the chemical analysis (Ernle et al., 2023; Monks et al., 2015). If O₃ remains in the sampling air, it can continue to react with other atmospheric compounds bearing O₃-reactive unsaturated functional groups during the collection, thus leading to sampling artefacts. Such O₃-induced artefacts have been long recognized in atmospheric science and especially aerosol sampling (Balducci et al., 2018; Grosjean, 1992; Van Vaeck & Van Cauwenberghe, 1984). In filter-based aerosol samplers, particles often reside on filters from several hours up to several days, providing enough time to react with O₃ of the sampling air streaming through filters and already collected particles (World Meteorological Organization (WMO), 2023). Consequently, collected particles may undergo oxidative reactions with O₃, resulting in distortion of their chemical composition.

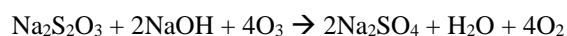
To mitigate O₃-induced sampling artefacts, upstream O₃ denuders or scrubbers are recommended for the sampling of particulate matter (e.g. PM_{2.5} and PM₁₀) by regulatory standards such as CEN EN 15549:2008. Particularly for O₃-reactive species like PAH (European Committee for Standardization (CEN), 2008), those denuders are used to remove O₃ from the sampling air stream and thereby prevent O₃ induced reactions on the filters before analysis.

There are different materials which have been deployed in O₃ denuders, which offer various mechanisms to scrub O₃ (Fick et al., 2001). Common approaches include potassium iodide (KI) coatings, manganese dioxide (MnO₂) catalysts, activated carbon (charcoal) adsorbents, silver-coated surfaces, and sodium thiosulfate (Na₂S₂O₃) impregnation (Ernle et al., 2023; Fick et al., 2001; K. Liu et al., 2014; Williams & Grosjean, 1990).

KI based denuders remove O₃ via stoichiometric redox reactions, thereby iodide oxidation products are generated. But the release of those reactive by-products such as I₂ and OH⁻, could interact with the atmospheric samples. For example, iodinated compounds and hydroxide from KI based O₃ scrubbers have been shown to degrade derivatization agents that might be used during the extraction procedure, and introduce secondary artefacts in sampling of carbonylic compounds (Ho et al., 2013).

MnO₂-coated denuders function via catalytically O₃ removal and have proven to prevent O₃ induced reactions of organic marker compounds in particulate matter. Yet, studies showed, that the strong oxidizing surface of the MnO₂ coated denuders itself can react with components of the sampling air. In particular, while the use of a MnO₂ denuder prevented the loss of particle-bound PAH during sampling, it also led to degradation of some PAH and concurrent formation of oxygenated PAH on the denuder surface (Y. Liu et al., 2006). Activated carbon and silver traps offer broad O₃ removal through adsorption or catalysis, but these materials are relatively non-selective and thus may adsorb other gas-phase species or alter trace constituents in the sampling air (Fick et al., 2001; Helmig & Greenberg, 1995; Liffick, 1970). In contrast, Na₂S₂O₃ offers a well-characterized stoichiometric reaction with O₃ yielding in unreactive inorganic products.

75 Thiosulfate reacts with O₃ via stepwise oxidation, yielding tetrathionate and, under excess O₃, sulfate as stable products. The reaction effectively removes O₃ without generating gaseous radical by-products (equation 1, Takizawa et al., 1973):



80

Na₂S₂O₃ coated denuders (TSOD) have been successfully employed in gas-phase sampling to protect analytes (e.g. volatile organic compounds, VOC, such as terpenoids and carbonyls) from O₃ reactions. In one comparative study, both KI and Na₂S₂O₃ O₃ filters achieved >90% removal efficiency for about 50 ppbV O₃, although KI showed slightly higher performance and less humidity sensitivity. For Na₂S₂O₃, O₃ removal increases with relative humidity (HRH) and declines in very dry air, while robust elimination is obtained at ~50–80% HRH (Rynek et al., 2025). Crucially, unlike KI, the thiosulfate method does not introduce organic reactive by-products, offering a potential advantage for preserving the organic composition of particle samples (Fick et al., 2001). Despite that, sodium thiosulfate O₃ denuders have seen little application in particulate-matter sampling compared with established O₃-denuders to date, and their performance in that context remains largely unexplored.

90 This knowledge gap is particularly relevant for ultrafine particles (UFPs, diameter < 100 nm), which are of special interest due to their many, diverse sources and health implications (Balmes & Hansel, 2024; Haddad et al., 2024; Li et al., 2023; Marval & Tronville, 2022). Among others, UFP distinguish from coarser particles because of their small mass, high number concentration and high surface-area-to-mass ratio and high diffusional mobility. Thus, UFPs can readily adsorb gases, like O₃ and other oxidants, and undergo rapid surface chemistry. These properties not only facilitate heterogeneous reactions, altering particle composition, but also influences toxicological behaviour (Kwon et al., 2020; Oberdörster et al., 1992).

95 A particularly relevant example is the enrichment of polycyclic aromatic hydrocarbons (PAH) in UFP. PAH are ubiquitous environmental pollutants originating from anthropogenic activities such as biomass burning and fossil fuel combustion (Abdel-Shafy & Mansour, 2016). They are of concern due to their persistence, potential for long-range transport, and the formation of toxic transformation products in the atmosphere (Ravindra et al., 2008). Their atmospheric lifetime and toxicity profiles are

100 governed by multiphase oxidation pathways involving gas-phase radicals and O₃. Among others, the higher-molecular-weight PAH (≥5 rings; benzo[a]pyrene (BaP), benzo[b]fluoranthene (BbF), benzo[k]fluoranthene (BkF), indeno[1,2,3-cd]pyrene (IcdP), together with four-ring PAHs such as chrysene (Chry) and benz[a]anthracene (BaA), are known to undergo heterogeneous ozonolysis on particle surfaces, especially under conditions of elevated O₃ exposure (Ji et al., 2024).

Another prominent example is N-(1,3-dimethylbutyl)-N'-phenyl-p-phenylenediamine (6PPD), a widely used tire antiozonant
105 that protects rubber surfaces through reactive scavenging of O₃. During tire wear, 6PPD is released into the environment and oxidized via O₃ to 6PPD-quinone (6PPDq). This transformation product has recently shown to exhibit acute aquatic toxicity, particularly toward coho salmon (Hu et al., 2022 ; H. N. Zhao et al., 2023).

A further compound class of interest are biogenic organic acids (bOAs), secondary oxidation products of monoterpenes that serve as markers for biogenic secondary organic aerosol (SOA) formation and ageing (Christoffersen et al., 1998; et al., 1998;
110 Denjean et al., 2015; Mutzel et al., 2016). This includes pinic acid (PA), pinonic acid (POA), terpenylic acid (TPA), and terebic acid (TA), which span a broad range of volatility: while PA is mainly particle-bound, POA, TPA, and TA remain partly in the gas phase (Kristensen, Bilde, et al., 2016; Yu et al., 1999). Because of their semi-volatile nature, non-specific adsorption of gas-phase bOAs or disturbance of the gas-particle equilibrium are known artefact pathways in denuder-based sampling, which can alter the measured particle-phase concentrations (Subramanian et al., 2004; Yatavelli et al., 2014; Yatavelli et al., 2012).
115 This issue is particularly relevant for UFP sampling, where the high surface-area-to-mass ratio enhances adsorption and desorption processes and thus amplifies potential denuder artefacts (Kristensen, Watne, et al., 2016; Kuwabara et al., 2016; Shiraiwa et al., 2011).

Given the emerging significance of UFP as important contributors to air pollution in atmospheric chemistry and human health,
120 being linked to oxidative stress, respiratory and cardiovascular diseases (Das et al., 2024; Pantzke et al., 2023), such artefacts can bias the interpretation of UFP chemical composition and reactivity, underscoring the need for artefact-free sampling when assessing their environmental and health relevance (Schraufnagel, 2020).

To address this, we designed a study combining laboratory and field experiments to assess the performance of TSOD for UFP
125 composition analysis under controlled and ambient conditions. Specifically, we focused on three representative classes of marker compounds: (1) PAHs to quantify O₃-induced losses; (2) tire-derived N-(1,3-dimethylbutyl)-N'-phenyl-p-phenylenediamine (6PPD) and its quinone (6PPDq) as a parent-product pair indicative of in-sampler ozonation; and (3) biogenic organic acids (bOAs) to test the selectivity and potential disturbance of gas-particle equilibrium.

130

2. Methods

135 2.1. O₃ denuder preparation

As O₃ denuder body, we used ceramic bodies (Ø 25.4 x 50 mm; squared channels with 400 cells per square inch, Rauschert, Germany) that were impregnated with Na₂S₂O₃ (Merck, 99%). Before coating the ceramic bodies, they were heated to 500 °C for 5 h, then cleaned in water (H₂O, obtained from Seralpur PRO 90 CN system with Supor DCF filter, Electronics Grade, 0.2 µm), subjecting them to ultrasonication for two cycles, each for 10 minutes. Subsequently, the bodies were manually dried with vigorous shaking ~~to remove bulk water from the honeycomb channels, to ensure the complete removal of water.~~ Next, the bodies were placed in a 5.6 mol L⁻¹ solution of Na₂S₂O₃ and H₂O, and ultrasonicated for an additional 10 minutes. ~~After ultrasonic impregnation, excess solution was removed by vigorous shaking while holding the monolith vertically to allow drainage of bulk liquid from the honeycomb channels. Afterwards, bulk solution within the channels, which was not removed by shaking, was~~ ~~It was imperative to thoroughly dry the denuders again with shaking and~~ blow-dried ~~it~~ with nitrogen (N₂, 145 99.99%). This was a critical step to prevent the growth of crystals within the ceramic matrix and the subsequent occlusion of the channels. The drying process was finished by baking the TSODs at a temperature of 120°C for a duration of 60 minutes. For ~~storage~~ ~~equilibration~~, the TSODs were placed in a sealed container with a separate water reservoir at the base to maintain a high humidity environment. This setup was left to rest overnight, for 12 hours, to achieve an even coating of Na₂S₄O₃ on the ceramic body. Afterwards the TSODs were stored under N₂ atmosphere in a closed glass vessel.

150

2.2 Laboratory test-bed for determining the denuder efficiency for O₃ removal under controlled conditions

To assess the O₃ removal efficiency of the TSODs, we set up an experimental test-bed in the laboratory. O₃ was produced in variable levels with a generator (Teledyne, T750U), diluted with zero air at a flow rate of 4 L min⁻¹, and passed through the TSOD. Upstream of the TSOD, humidified air was added to the sample flow by bubbling 4 L min⁻¹ of zero air through a suction flask filled with H₂O, yielding a total flow of 8 L min⁻¹ through the TSOD (Fig. 1a). We measured the ~~relative humidity~~ ~~(RH)~~ upstream of the TSOD, which remained constant at about 50%. Downstream of the TSODs, the O₃ mixing ratio was measured using an O₃-analyzer (Thermo Scientific, MLU, Model 49i). We tested the TSOD for a range of O₃ mixing ratios of 5 to 200 ppbV. ~~To assess the practical zero-level response of the instrument, separate zero-air measurements were performed, yielding an analyzer signal of 4.6 ± 0.5 ppbV under O₃-free conditions.~~

160

2.3 Assessment of particle losses within the O₃ denuder

To examine potential particle losses due to the TSOD, we conducted loss tests with simulated atmospheric organic aerosol (SimOA) using the Bayreuth Atmospheric simulation Chambers (BATCH). To maintain a stable aerosol mixture for several hours, we flushed the 700L cylindrical glass chamber with ambient air for several hours. Subsequently, 0.05 mL of alpha-pinene (≥98,0 %, Carl Roth) was injected into the airflow, while a nebulizer delivered seed particles (from spraying saturated

ammonium sulfate solution and drying) into the chamber at a flow rate of 3 L min^{-1} for 3 minutes. After an additional 5 minutes, the pump supplying ambient air was switched off, and the solar simulator (UV Osram HMI, 4000 W, filtered with a water-cooled glass plate) (Ofner et al., 2011; Z. Zhao et al., 2008), was ignited for 15 minutes to produce first O_3 and subsequently SimOA. We connected three TSOD bodies in line to the chamber. Downstream the TSOD, a Y-connector was attached splitting the flow into two channels. One channel end led to a pump which allowed to adjust to variable flows through the denuder ($4\text{-}30 \text{ L min}^{-1}$). The other channel end led to a particle size spectrometer to record the particle size distribution after the TSOD (Cambustion, DMS500). As a control, the setup was also operated without the TSOD installed in the stainless-steel cylinders.

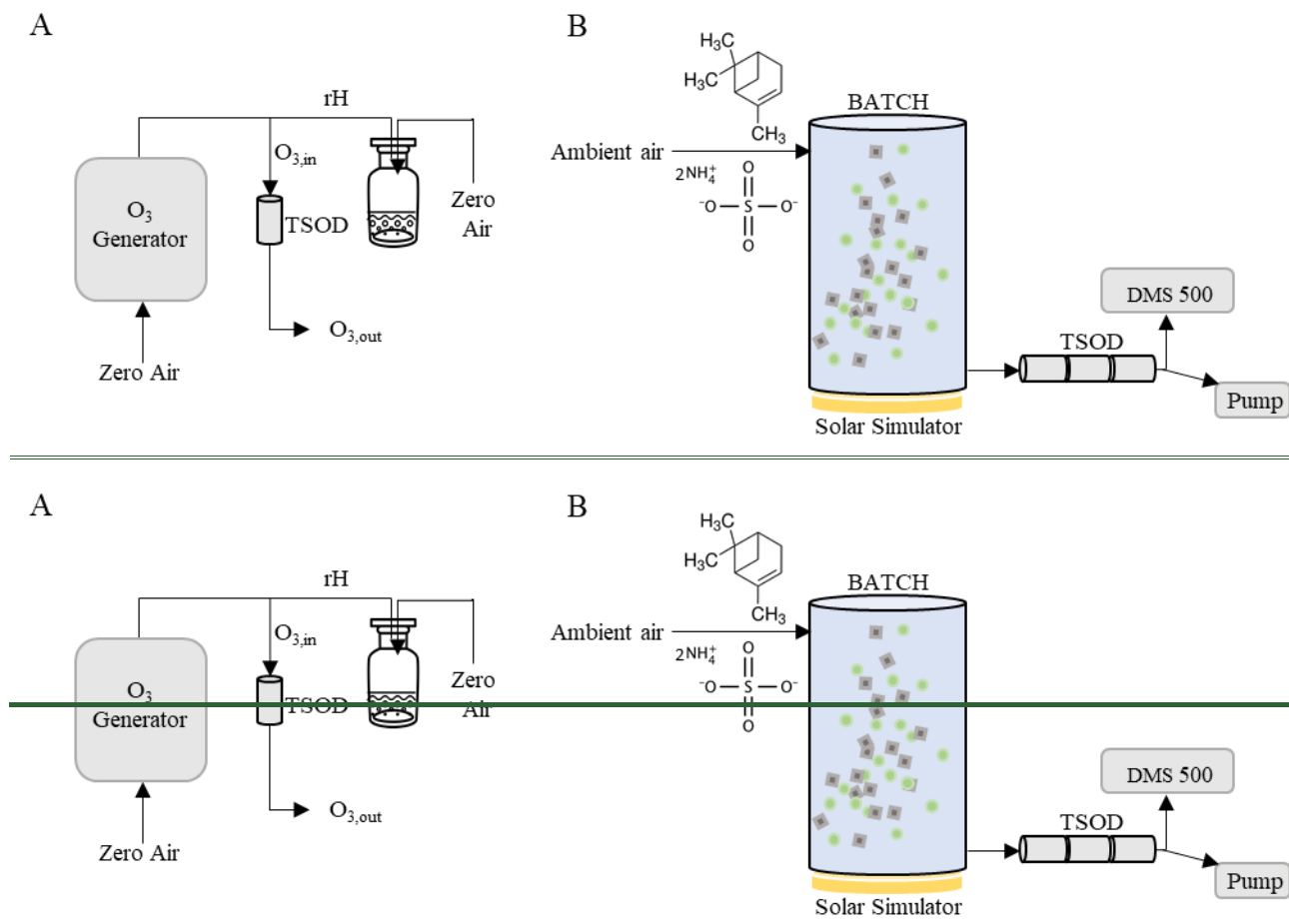


Figure 1 Schematic of the laboratory test-bed for assessing the O_3 removal efficiency (A) and potential particle losses of TSODs (B). (A) O_3 was generated, diluted with zero air, humidified to $\sim 50\%$ relative humidity, and passed through the TSOD. Downstream O_3 concentrations were measured using an O_3 analyzer. (B) For particle loss tests, the setup was connected to the BATCH, where SimOA was generated from α -pinene oxidation with ammonium sulfate seed particles and ambient air. The aerosol flow was directed through three TSODs, and particle size distributions were measured downstream using a DMS500.

2.4 Field deployment and UFP sampling for offline chemical characterization

185 To evaluate the performance of the TSOD under real environmental conditions, a novel setup was installed in a measurement
container at an urban field site of the University of Applied Sciences in Augsburg, Germany (48.35⁸⁷⁹⁴⁷° N, 10.907⁰⁹⁰° E)
in September 2023. The site is dominated by domestic heating and traffic which are a likely sources for PAH and 6PPD/6PPDq.
Streetside and campus vegetation emitted monoterpenes, providing biogenic precursors for SOA. Air was drawn through a
PM10 sample inlet from the roof of the air-conditioned container at a height of 4.2 m. A stainless-steel sampling tube (2.1 m
190 x 28 mm) led into the container, where it was connected to a modified 120 R Microorifice Uniform Deposit Impactor (MOUDI,
TSI). The 120R-MOUDI was reduced to sample with cut-off sizes of 2.5, 1.0, and 0.1 µm. The impactor plates were coated
with high-vacuum grease to minimize bounce effects. Behind the reduced MOUDI unit, the After Filter Stage, intended to
collect particles smaller than 0.1 µm, was omitted, and instead, a Y-connector (30 cm x 28 mm) was installed, leading to an
automated filter changer (HYDRA Dual Sampler, FAI instruments), thereby introducing a two-channel filter collector. Here,
195 UFP samples were collected from both channels in parallel on pre-baked quartz fiber filters (47mm Whatman, QM-A) and,
following a weekly change, stored at -20°C in analyslides (Cytiva) until analysis. In one of these channels (Channel A), the
TSOD was installed, while the other channel (Channel B) was operated with an uncoated ceramic body as reference ([Figure
S1 and S2](#)). For control measurements, both channels were operated with a ceramic body without coating. The total flow
through the impactor was set to 30 L min⁻¹ according to the manufacturer's specifications, with a corresponding collection of
200 15 L min⁻¹ per channel. Ambient O₃ concentrations were measured after channel A (41M, UV Photometric O₃ analyzer, ansyco,
environment s.a) and cross-checked against values reported by the local governmental monitoring station (Landesamt für
Umwelt, LfU). This field setup intended to serve: (i) as assessment of the O₃ removal efficiency under real-world conditions
over a longer time period, and (ii) the effect of O₃ removal during collection of UFP samples for subsequent offline chemical
analysis.

205

2.5 Chemical marker compounds

UFP samples obtained during the field campaign were analyzed offline to investigate the effect of upstream O₃ removal via
TSOD on the concentrations of selected organic marker compounds. The following target compounds were analyzed: (i) PAHs:
BaP, BbF, Bk, IcdP, Chry, and BaA; (ii) parent-product (ozonolysis) pair: 6PPD and 6PPDq; and (iii) bOAs: PA, POA, TPA,
210 and TA. Internal standards were 3-methylcholanthrene (3-MC, Merck, 98.0 %, 0.4 µM) and nicotinic acid (NA, Merck, 99.5%,
10 µM). Reagents, solvents, and standards were sourced from LGC Standards, Merck, Carl Roth, ASCA-Berlin, and Fisher
Chemical (purities >95–99.99 %). HPLC-grade acetonitrile (ACN, 99.95 %), methanol (MeOH, 99.99 %), water (H₂O;
Seralpur PRO 90 CN, electronics grade, 0.2 µm), and formic acid (HCOOH, ≥98%) were used as mobile-phase components;
dichloromethane (DCM, 99.8 %) and high-purity nitrogen (N₂, 99.999 %) were used for extraction/solvent handling and
215 evaporation.

2.6 Extraction

We extracted the selected marker components from the filters via a soft, solvent-based and optimized protocol: (1) the filter loaded with particles was divided into two equal parts. One part was extracted, the other one used as backup. (2) The filter-half for extraction, was spiked with 50 μL of each internal standard, namely 3-methylcholanthrene (3-MC, 0.4 μM) and Nicotinic acid (NA, 10 μM) and cut into small fragments. (3) These filter fragments were then transferred into a glass container with a screw cap, and 2 mL of extraction solvent (e.g. analytical-grade dichloromethane (DCM, Fisher Chemical, 99.8%) and methanol (MeOH, Carl Roth, $\geq 99.9\%$)) were introduced. (4) The samples underwent extraction through agitation within a closed flask for a duration of 15 minutes using a vortex shaker (2000 rpm). (5) Filter residues were kept in the glass container. Extracts were filtered using custom-designed glass frits with a diameter of 1 cm and a pore size of 20 μm to filter any potential filter residue.

Steps (3) to (5) were repeated three times, each time employing a different extraction solvent. The sequential solvents used were, in order, pure MeOH, 50:50 MeOH:DCM, and pure DCM. Subsequently, the solvent from the combined extracts was evaporated under a gentle flow of nitrogen while cooled with ice to avoid loss of semi-volatile compounds. A droplet was kept as residue which was dissolved in 1 mL of a 60:40 solution of acetonitrile (ACN, Carl Roth, 99.95%) and Millipore water (H_2O obtained from Seralpur PRO 90 CN system with Supor DCF filter, Electronics Grade, 0.2 μm). This was transferred into two separate vials for subsequent analysis. Throughout this entire sample preparation process, the samples were consistently stored in an ice cooled environment to avoid losses.

2.7 HPLC methods

The extracts of the collected UFP were analyzed using two complementary high-performance liquid chromatography (HPLC) systems, adapted to the specific analytical requirements of the target compounds. PAHs were quantified using an Agilent 1260 Infinity system equipped with a fluorescence detector (Agilent 1100 Series FLD). bOAs and tire-derived antioxidants, including 6PPD and its transformation product 6PPDq, were analyzed on an Agilent 1100 Series HPLC coupled to an electrospray ionization mass spectrometer (ESI-MS; Agilent 6130 Single Quadrupole).

All analyses were conducted using HPLC-grade solvents: acetonitrile, ultrapure water, and formic acid ($\geq 98\%$, Carl Roth). Chromatographic separation and detection settings were optimized for each compound class. A detailed summary of the applied methods is provided in our previous publication and in the SI (Eckenberger et al., 2025; Table S1).

To assess the overall analytical recovery, spiking experiments were performed in triplicate. One half of a pre-baked quartz fiber filter (47 mm, Whatman QM-H) was spiked with 10 μL of a 10 μM standard solution containing all target compounds and subsequently extracted following the same procedure used for ambient samples. Recoveries were calculated using external calibration and expressed as the ratio of measured to expected concentrations:

$$Rec = \frac{c_{measured}}{c_{expected}} \times 100 \quad (2)$$

250

Average recoveries ranged from 70 % to 101 % and were consistent across compound classes. Specifically, recoveries for PAHs were 78 ± 5 % for BaP, 74 ± 4 % for BbF, 89 ± 6 % for BkF, 70 ± 4 % for IcdP, and 97 ± 5 % for Σ Chry+BaA. 6PPD and its transformation product 6PPDq yielded recoveries of 75 ± 7 % and 81 ± 7 %, respectively. Among the bOAs, PA was recovered at 84 ± 6 %, while POA, TA, and TPA showed recoveries of 101 ± 6 %, 85 ± 6 %, and 96 ± 6 %, respectively.

255 Uncertainties represent 1 σ standard deviations (SD) obtained from triplicate spiking experiments.

To account for analyte-specific losses, all sample concentrations were corrected for recovery using the following equation:

$$260 \quad c_{\text{sample}_{\text{corrected}}} = c_{\text{sample}_{\text{measured}}} \times \left(\frac{100}{\text{Rec}} \right) \quad (3)$$

Validation of the analytical procedure was performed using the NIST Standard Reference Material SRM 2786 (Fine Atmospheric Particulate matter with mean diameter <4 μm), which was applied to a quartz filter and processed identically to the environmental samples. Specifically, 107 ± 4 % of the certified BaP concentration was recovered. BbF, BkF, Σ (Chry +
265 BaA), and IcdP showed recoveries of 96 ± 5 %, 94 ± 7 %, 89 ± 5 %, and 99 ± 7 %, respectively. The results agreed with the certified concentrations within their stated uncertainty, confirming the reliability of the method even in the presence of a complex particulate matrix. Limits of detection (LOD) were determined for each compound from four replicate injections of a diluted calibration standard, targeting a signal-to-noise ratio of 3. The LOD was calculated as:

$$270 \quad \text{LOD} = \frac{3 \times \sigma}{\text{RF}} \quad (4)$$

where σ is the standard deviation of replicate peak areas and RF denotes the compound-specific response factor derived from external calibration. For comparison with ambient concentrations, airborne detection limits LOD_{Air} were calculated by normalizing the LOD to the sampling volume (Table S2).

275

Instrument and field blanks were routinely collected and processed alongside samples using the identical preparation. Instrument blanks consisted of pure-solvent injections between runs. Field filter blanks were prepared by placing clean quartz filters in the sampler holders but without drawing air. Blank signals were subtracted on a per-compound basis when reproducible across replicate blanks and clearly below sample signals. If blank values varied strongly within a batch or exceeded expected background levels, affected samples were excluded from further analysis.

280

Last step to calculate mass concentrations of the marker compounds in UFP was to convert the blank-corrected extract concentrations to air concentrations by multiplying the corrected concentration by the final extract volume (1 mL), correcting

for recovery and the analyzed filter fraction (only half filter was analyzed), and normalizing to the sampled air volume (21.6 m³).

285

3. Results and Discussion

3.1 Laboratory evaluation of denuder performance

To evaluate the O₃ removal efficiency of the TSOD under controlled conditions, we first conducted a laboratory test. Previous studies have shown that ~~HRH~~ plays a critical role in the reactivity of sodium thiosulfate toward O₃ (Ernle et al., 2023). Specifically, at 80% ~~HRH~~, the lifetime of the sodium thiosulfate scrubber increases dramatically, enabling complete O₃ removal from the sample air, in contrast to its performance under dry conditions. As a reference for typical ambient conditions at our field site in Augsburg, daily data from the nearest German Weather Service (Deutscher Wetterdienst, DWD) climate station for the meteorological summer 2023 yield an average ~~Relative humidity~~ of 69 % ± 11 % (Data source: DWD). We therefore intentionally conducted our laboratory experiments under distinctly drier conditions (~~reported as HRH = 52.4–53.3 %~~), in order to test TSOD performance near the lower end of the humidity range expected during field operation, ~~where the scrubber is known to be less efficient. Previous studies indicate that thiosulfate-based ozone removal decreases under drier conditions, consistent with reduced water availability at the denuder surface~~ (Ernle et al., 2023; Rynek et al., 2025)

290
295

In urban and suburban environments, O₃ levels frequently peak between 70 to 100 ppbV and can surpass 120 ppbV during intense pollution events (Bell et al., 2007; Cooper et al., 2014; WHO, 2021). Thus, the inlet O₃ mixing ratio was incrementally increased to up to 200 ppbV ~~in a sequence of discrete measurement intervals~~. As depicted in Figure 2, the outlet O₃ mixing ratio ~~(4.4–5.0 ppbV) were indistinguishable from this zero-air baseline, indicating that ozone downstream of the denuder was below the practical detection limit of the measurement setup~~ ~~remained consistently between 0 and 0.3 ppbV~~.

300

This indicates that, even at comparably high mixing ratios, O₃ was removed from the air in this experimental setup. However, it is important to note that this experiment was conducted under controlled laboratory conditions with constant temperatures, ~~HRH~~, and zero air. Furthermore, the duration of the experiment does not match the typical collection duration required for UFP, which, due to their low mass, must be collected over several hours or days for mass-based chemical analysis. To complement the controlled laboratory evaluation, a field deployment was conducted to assess the TSOD's applicability under real-world sampling conditions. The results of this field implementation, including performance under ambient O₃ exposure and implications for UFP sampling, are discussed in detail in Section 3.2.

305

310

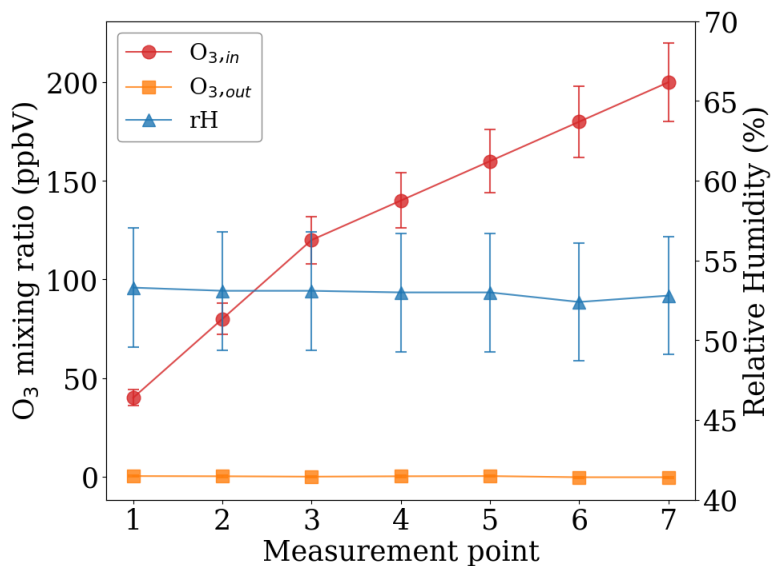


Figure 2 Average O_3 mixing ratios upstream (“ $O_{3,in}$ ”, red) and downstream (“ $O_{3,out}$ ”, orange) of the TSOD during consecutive laboratory measurement intervals with stepwise increasing under-controlled laboratory conditions for varying inlet O_3 mixing ratios (40–200 ppbV). Relative humidity (rH) was simultaneously monitored and remained constant. Lines are included to guide the eye.

315

To assess if the sampling flow channelled through the TSOD is associated with particle losses, we compared particle number concentrations (PNC) measured with (wTSOD) and without (woTSOD) TSOD installed, where the woTSOD setup served as the reference using an empty TSOD housing. The analysis was performed for two particle size ranges: 10–100 nm and 10–
 320 1000 nm. All measurements were repeated at three flow rates (4, 11, and 30 L min⁻¹), and an instrument uncertainty of 10 % was assumed. In the 10–100 nm range, relative differences between the wTSOD and woTSOD configurations ranged from 2 % to 7 % depending on the flow rate. At 4 L min⁻¹, the difference corresponded to a 2 % loss, increasing to 7 %, and 6 % at 11 L min⁻¹ and 30 L min⁻¹, respectively.

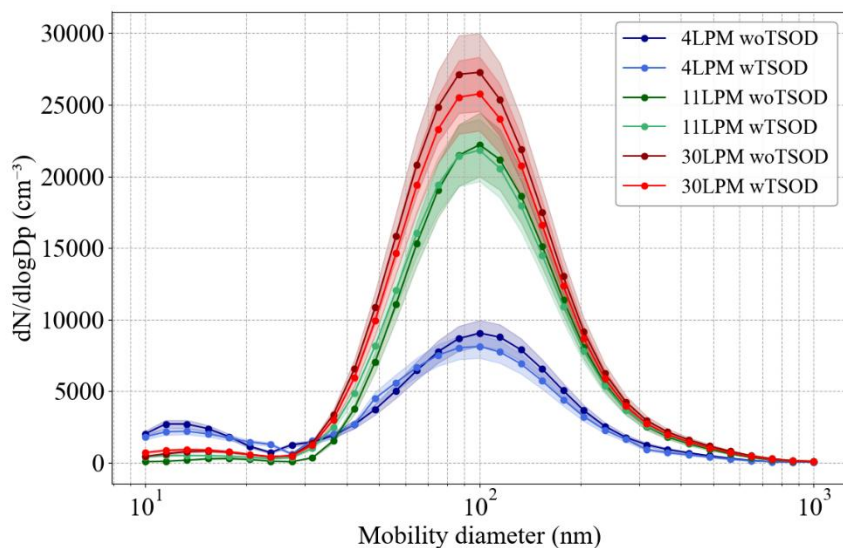
320

Comparable results were obtained for the full-size spectrum (10–1000 nm). Measured losses amounted to 7 % (4 L min⁻¹), 3 %
 325 (11 L min⁻¹), and 6 % (30 L min⁻¹) (Fig. 3).

325

The average observed deviation between the wTSOD and woTSOD measurements was 5% and falls within the measurement uncertainty of the particle size spectrometer utilized. Hence, we found no significant losses in particle number concentrations and the TSOD setup can be considered suitable for ambient UFP sampling. Since the measurements at 30, 11, and 4 L min⁻¹ were conducted sequentially, the absolute particle number concentrations between the different flow-rate experiments vary and are not directly comparable.
 330

330



335 **Figure 3 Particle size distributions recorded downstream of the TSOD and for reference without a TSOD at three different flow rates (4, 11, and 30 L min⁻¹). Blue tones refer to 4 L min⁻¹ (royal blue: wTSOD, dark blue: woTSOD), green tones to 11 L min⁻¹ (MediumSeaGreen: wTSOD, dark green: woTSOD), and red tones to 30 L min⁻¹ (red: wTSOD, dark red: woTSOD). Shaded areas represent ±10% uncertainty.**

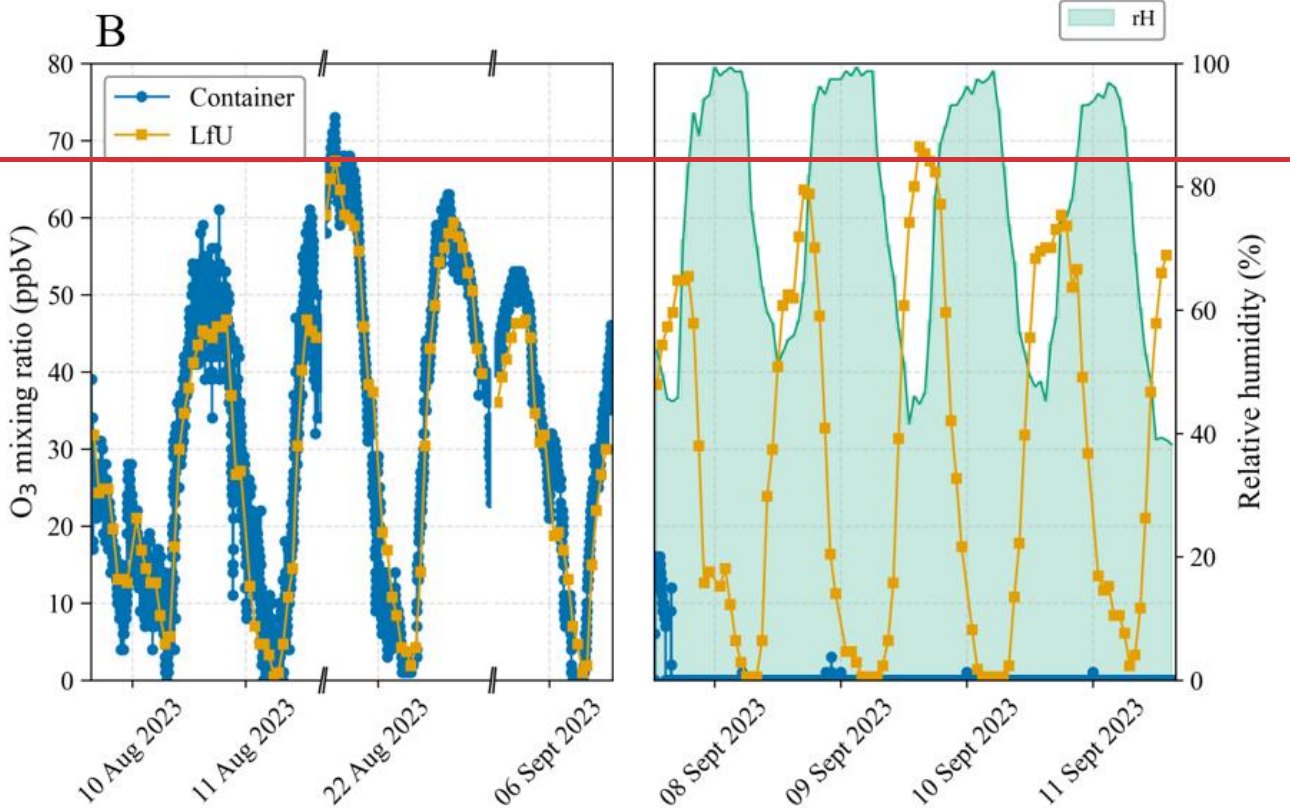
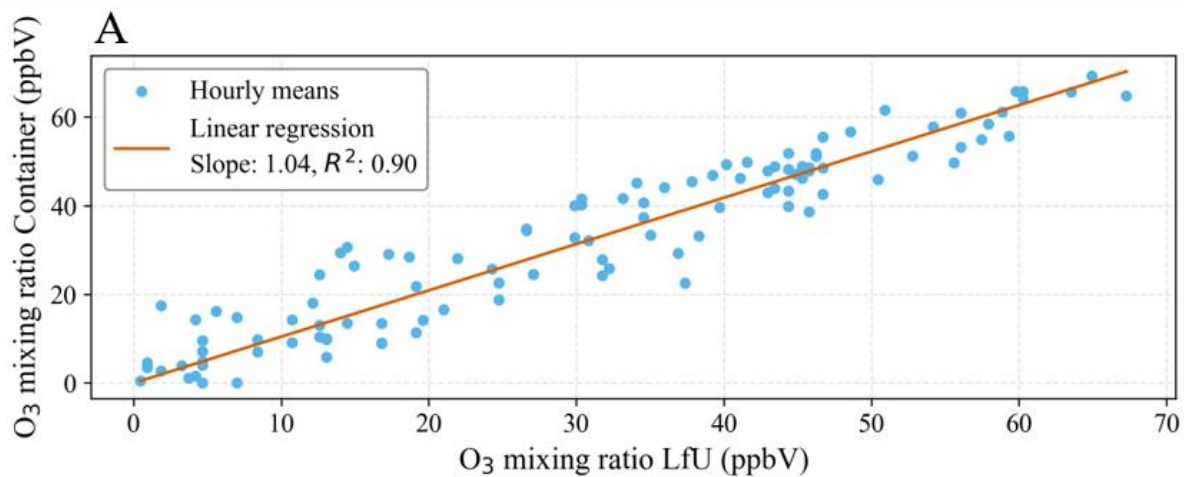
3.2 Field performance of the denuder and chemical composition of UFP

The O₃ removal performance of the TSOD was further evaluated under ambient conditions during a five-day deployment at an urban field site. Due to the lack of a second O₃ analyzer, the experiments were conducted using only one device. Initially, measurements were taken with the O₃ analyzer without the installed coated ceramic body. Subsequently, these measurement results were compared with publicly available data on O₃ concentrations from a nearby site monitored by the Bavarian Environment Agency (Bayerisches Landesamt für Umwelt (LfU). LÜB – Messwertarchiv: O₃, hourly data, station Augsburg/LfU, 8th August until 13th September 2023. Accessed 8th June 2025).

345 The hourly averaged data are compared in Figure 4a. A linear regression yielded a slope of 1.04 and a coefficient of determination (R²) of 0.90, confirming the comparability of both datasets within the uncertainty of the measurement. Therefore, no correction was applied to either dataset before subsequent analysis.

350 During the period when a TSOD, in channel A of the measurement setup, was installed, the O₃ mixing ratio behind the TSOD was consistently measured. In comparison to the measurements from the Bavarian Environment Agency, it was observed that the O₃ mixing ratio behind the TSOD remained ~~at 0~~ **below the detection limit ppbV**, while the outdoor O₃ mixing ratios fluctuated between 0 and 65 ppbV (Fig 4b). Over the period of 5 days, the TSOD removed O₃ reliably from the sampled air.

These results indicate the O₃ removal efficiency of the TSOD under environmental conditions and over an extended time period.



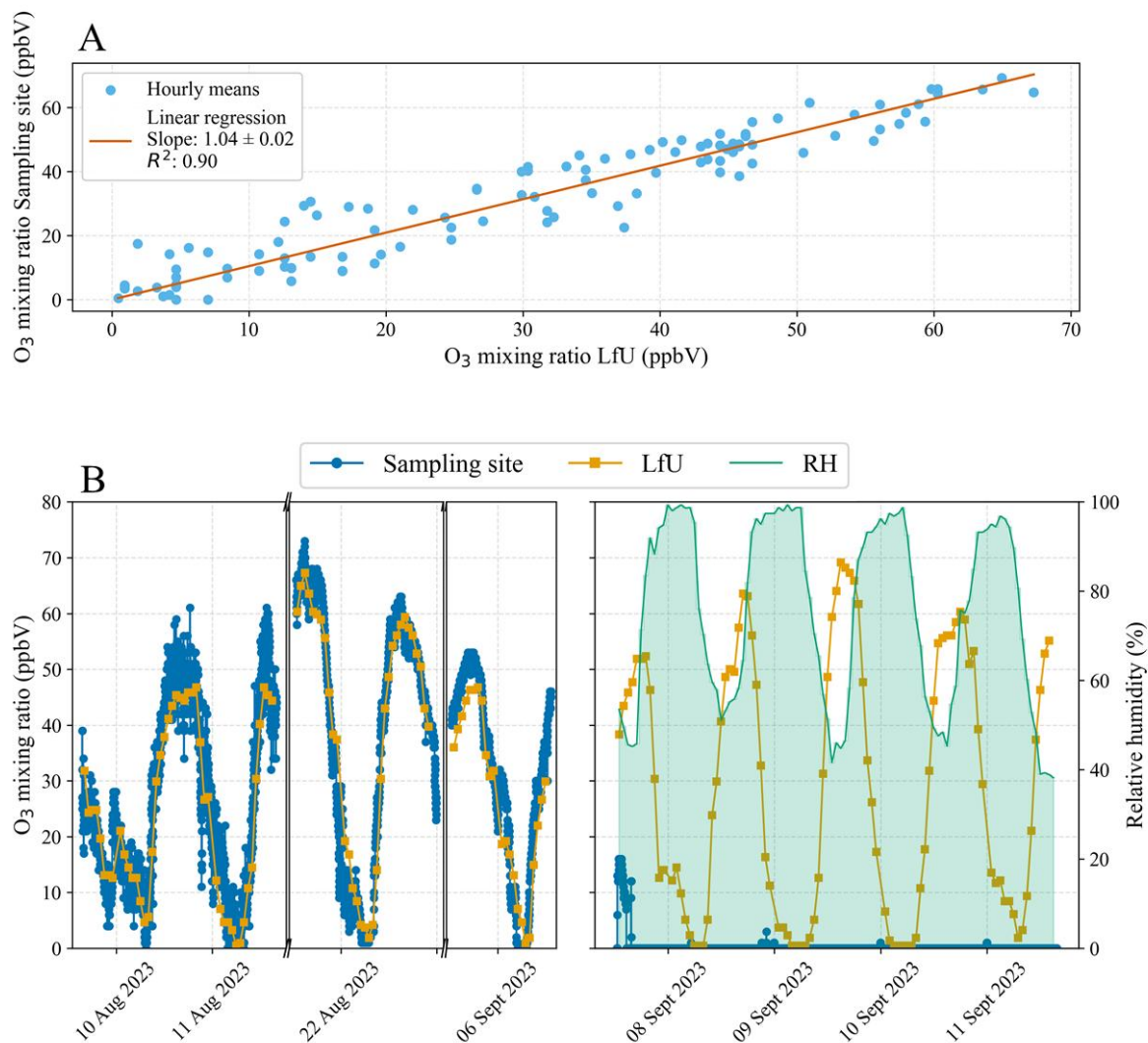


Figure 4 (A) Correlation between hourly averaged O₃ ~~concentrations~~ mixing ratios from the sampling site and the LfU monitoring station. A linear regression through the origin (red line) yields a slope of 1.04 and $R^2 = 0.90$. (B) Time line of ambient O₃ ~~mixing ratios~~ concentrations before and during the field campaign in Augsburg. Measurements before the campaign were taken from a setup without a TSOD, allowing comparison with reference data from the LfU monitoring station ~~Bavarian Environment Agency~~. After the start of UFP sampling, measurements were taken downstream of the TSOD (blue, "Sampling site") and compared to the LfU reference data (orange, "LfU").

360

365 3.2.2 Chemical organic tracer analysis of UFP

To assess the efficiency and selectivity of the TSOD under ambient conditions, we evaluated changes in particle-phase concentrations of selected organic tracer compounds. We analyzed representative compounds from three organic marker

groups: PAHs, 6PPD and 6PPDq, and bOAs. All compounds are potentially susceptible to TSOD-induced sampling improvements or artefacts. This could be either by prevented degradation through O₃ oxidation or by shifts in gas-particle partitioning through removal of gaseous components. In the following, we present compound-specific mass concentrations measured in Channel A (with O₃ removal via TSOD) and Channel B (without O₃ removal comparing to an uncoated ceramic body). We assess the TSOD performance for each class of marker compounds.

First, to verify the performance and internal consistency of the dual-channel sampling setup, all targeted marker substances were analyzed under reference conditions in which neither sampling line contained an upstream-coated ceramic body. The measured mass concentrations of all compounds in UFP sampled through Channel A and Channel B agreed within the uncertainties. Regression slopes were close to unity for PAHs (BaP: 0.97, BkF: 0.83, BbF: 1.18, IcdP: 1.05, ΣChry+BaA: 0.92), demonstrating the absence of systematic differences between the two channels. Similarly, mass concentrations of 6PPD (slope = 1.01) and 6PPDq (slope = 1.04) and the bOAs, including PA (slope=1.00), POA (slope = 0.94), TA (slope = 1.003), and TPA (slope = 1.010) were comparable for both channels (Table 1). Detailed regression plots are provided in the Supporting Information (SI) (Figures S2).

Deploying the TSOD in Channel A and regressing concentrations in Channel B (no O₃ removal) against Channel A provides a direct quantitative analysis of O₃ induced sampling artefacts. For PAHs, slopes of 0.54–0.85 (BaP: 0.60, BkF: 0.85, BbF: 0.66, ΣChry+BaA: 0.54, IcdP: 0.62; Table 1) indicate about 15 to 46 % in-sampler losses when O₃ is present (Fig 5a). For context, ambient BaP was on the order of about 9 pg m⁻³ with the deployment of a TSOD, without O₃ removal this would be 40 % lower. In contrast, 6PPD and its oxidation product 6PPDq show opposite behaviour (Fig. 5b, Table 1): 6PPD exhibits a slope of 0.52, indicating underestimation without O₃ removal, whereas 6PPDq shows a slope of 1.40, reflecting overestimation due to in-sampler ozonolysis. These findings are consistent with the oxidative conversion of 6PPD to 6PPDq, which is suppressed in-situ when O₃ is scrubbed from the sampling air. Mechanistic and computational studies have shown that O₃ attacks the aromatic amine moiety of 6PPD, forming hydroxylated intermediates that subsequently oxidize to 6PPDq as the major transformation product (Cataldo, 2019; Rossomme et al., 2023; H. N. Zhao et al., 2023). In our dual-channel approach, we find that about 13 to 20 % of the initial 6PPD was converted to 6PPDq. These transformation yields align with those reported by Zhao et al. (2023), who reported that 1–19 % of 6PPD was converted to 6PPDq during controlled ozonation of 6PPD.

Conversely, bOAs exhibited negligible inter-channel differences (slopes about 0.95 to 1.09, Fig 5c, Table 1), indicating that the TSOD effectively removes O₃ without perturbing gas–particle partitioning. Given their semi-volatile nature, any non-selective uptake or release by the TSOD would shift this equilibrium and drive evaporation or condensation, which is not observed (Kristensen, Bilde, et al., 2016; Yu et al., 1999). This indicates that the sodium thiosulfate coating does not disturb gas-particle equilibrium.

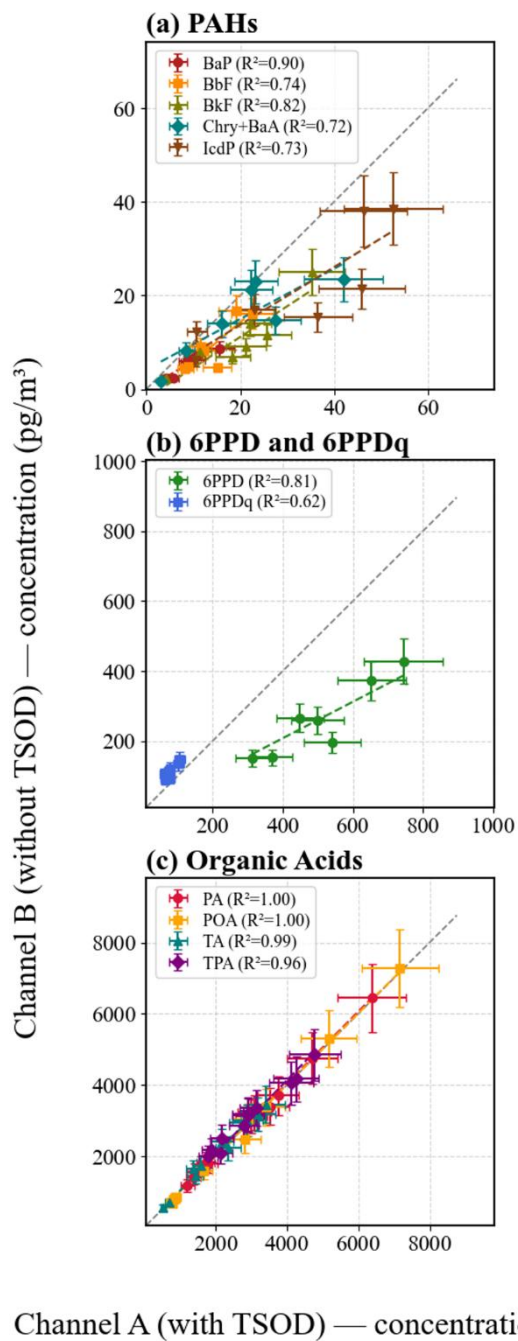
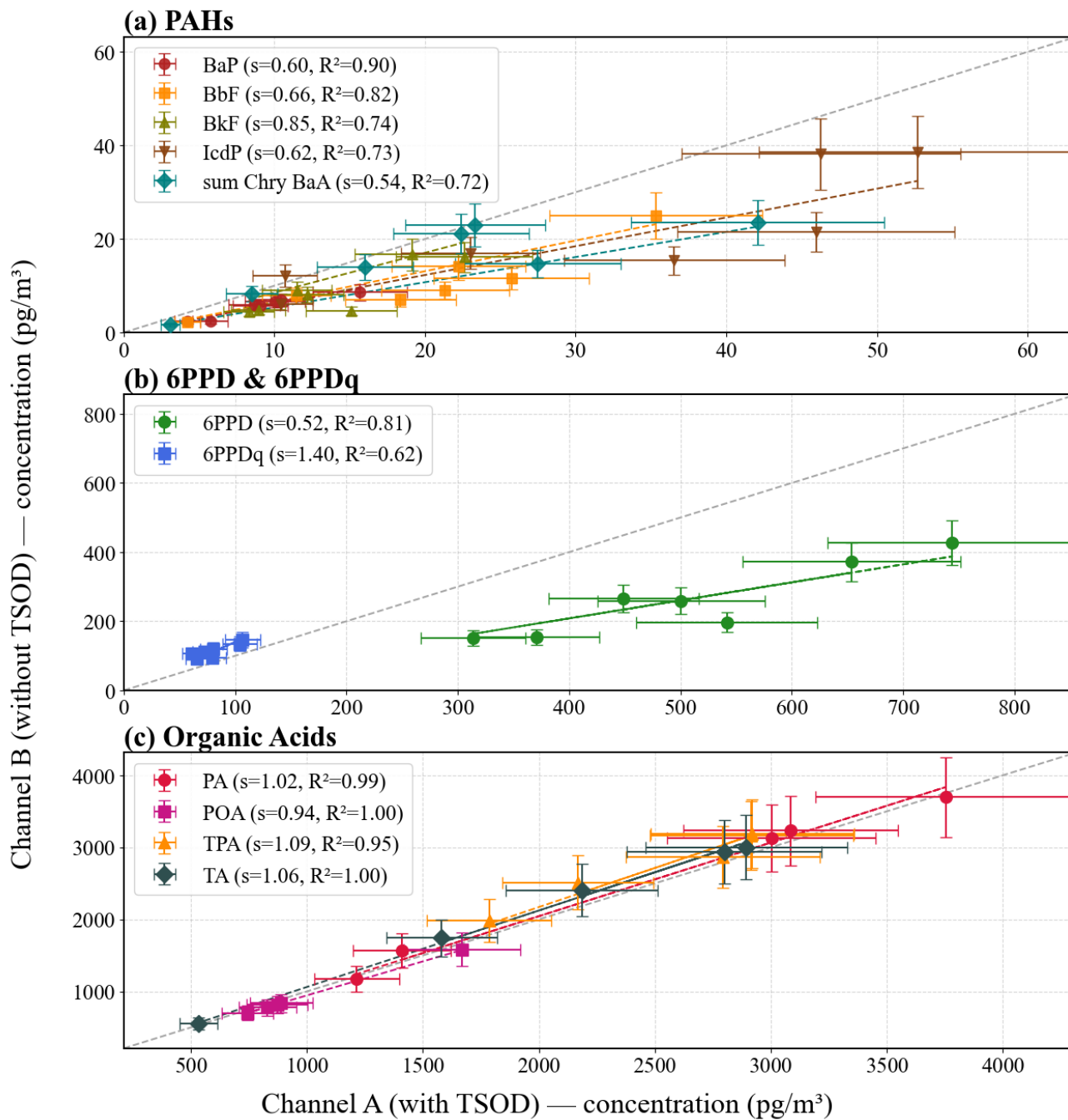


Figure 5 Comparison of analyte concentrations measured in sampling channel A (with TSOD, O_3 removed) and channel B (without TSOD, O_3 present). The sample in channel B was exposed to ambient O_3 mixing ratios during the 24hr sampling interval. Each data point represents the mass concentration of an analyte measured in parallel filters. Dashed lines show linear regressions constrained through the origin, while grey dashed lines represent the 1:1 relationship. (A) PAHs: BaP, BbF, BkF, IcdP, and sum Chry BaA. (B) Tire wear antioxidants and their transformation product: 6PPD and 6PPDq. (C) bOA: PA, POA, TPA, and TA. The standard deviation used for the error bars is derived from three replicate measurements of three extracted filter samples.



410

Table 1 Linear regression slopes of marker compound concentrations between the two sampling channels during operation with ozone removal (TSOD installed in Channel A). For comparison, slopes obtained during reference operation, when both channels were equipped with uncoated ceramic bodies, are also shown ~~marker compound concentrations between sampling channels for measurements with and without O₃ removal~~ (Reference, Figure S3). Slopes were derived from linear regressions constrained through the origin. Values greater or smaller than unity indicate enhancement or loss of the respective compound in the presence of O₃ removal.

Compound	Slope	
	Relative change due to O ₃ exposure during sampling	Reference
BaP	0.60	0.97
BbF	0.85	1.18
BkF	0.66	0.83
IcdP	0.62	0.98
Sum Chry BaA	0.54	0.92
PA	1.02	1.00
POA	0.94	1.01
TA	1.06	1.00
TPA	1.09	1.01
6PPD	0.52	1.01
6PPDq	1.40	1.04

415 Among the PAHs, the most pronounced O₃ related losses were observed for the sum of BaA Chrys (46 %) and for BaP (40 %), followed by IcdP (38 %), BkF (34 %), and BbF (15 %). These losses observed in the UFP fraction are consistent with sampling artefact studies focusing on O₃ related degradation in larger particle fractions.

For PM₁₀, Balducci et al. (2018) reported summer field BaP concentrations of about 0.022 to 0.028 ng m⁻³ and, in laboratory tests at 400 ppbV O₃ for 1–3 h, observed BaP losses of ~24–55% (with smaller losses for BbF and BkF). Similarly, Y. Liu et al. (2006) reported daily O₃ concentrations of 50–95 μg m⁻³ (≈ 25–48 ppbV at 290 K) and deployed a MnO₂ denuder into PM₇ sampling. The observed concentrations for particulate PAH rose from 0.16 to 0.20 ng m⁻³ (+25%) for BaP and shifts for BaA (-7%), chrysene (-14%), and IcdP (+6%), while BbF remained unchanged upon the removal of O₃. Consistently, the study of Liu et al. (2014) in Beijing summer showed averaged O₃ concentrations of 74.6 μg m⁻³ (~37 ppbV). They sampled PM_{2.5} with a denuder-equipped method, which yielded higher particulate PAH concentrations than the conventional setup (Σ₉PAH = 42.3 ± 10.5 vs 27.1 ± 13.8 ng m⁻³), and for BaP a corresponding underestimation from 49% to 83% without O₃ removal. While inter-channel artifacts such as gas-particle partitioning ("blow-on" or "blow-off") might occur, our control measurements

showed no inter-channel bias in the absence of the TSOD. Therefore, we conclude that the observed differences are primarily driven by O₃-induced chemical transformation of particle-bound PAHs in the channel without the denuder.

430

To contextualize the relative O₃-induced artefacts, we compared them with the heterogeneous pseudo-first-order rate constants (k') for O₃ loss of particle-bound PAHs reported by Bedjanian & Nguyen, (2010). In this study, soot from a premixed kerosene-air flame was exposed to an initial O₃ of 1.3×10^{12} molecules cm⁻³ (≈ 51.4 ppbV at 290 K) under dry, dark flow conditions. Figure 6 shows that our observed UFP degradation pattern generally follows the compound-specific reactivities described by Bedjanian & Nguyen (2010). Consistently with those compound-specific reactivities, our degradation pattern largely follows $\Sigma(\text{Chry} + \text{BaA}) > \text{BaP} \gtrsim \text{BkF}$. Quantitatively, $\Sigma(\text{Chry} + \text{BaA})$ shows the highest k' (7.3×10^{-3} s⁻¹), followed by BaP (6.8×10^{-3} s⁻¹) and BkF (6.0×10^{-3} s⁻¹). BbF has a comparable k' (5.5×10^{-3} s⁻¹), about 80% of BaP, yet its O₃-related loss in our data is only ~40% of BaP. This discrepancy likely reflects particle-phase microphysics, specifically the partial embedding or molecular shielding within condensed organic matrices. These structural factors inherently reduce the effective surface accessibility of certain PAHs (Kwamena et al., 2007; Shiraiwa et al., 2011; Zhou et al., 2019). Furthermore, the elevated ~~Relative humidity~~ during sampling (74–84 %) may have further enhanced this effect, by increasing particle viscosity or forming hydrated amorphous surface layers which can act as transient diffusion barriers (Pöschl et al., 2001). Consequently, while the relative ranking of O₃ susceptibility among PAHs in UFP is preserved, the overall magnitude of degradation is likely strongly influenced by particle-phase microphysics. This distinction underscores the critical importance of integrating such particle-phase effects when extrapolating laboratory kinetic data to realistic atmospheric conditions.

435
440
445

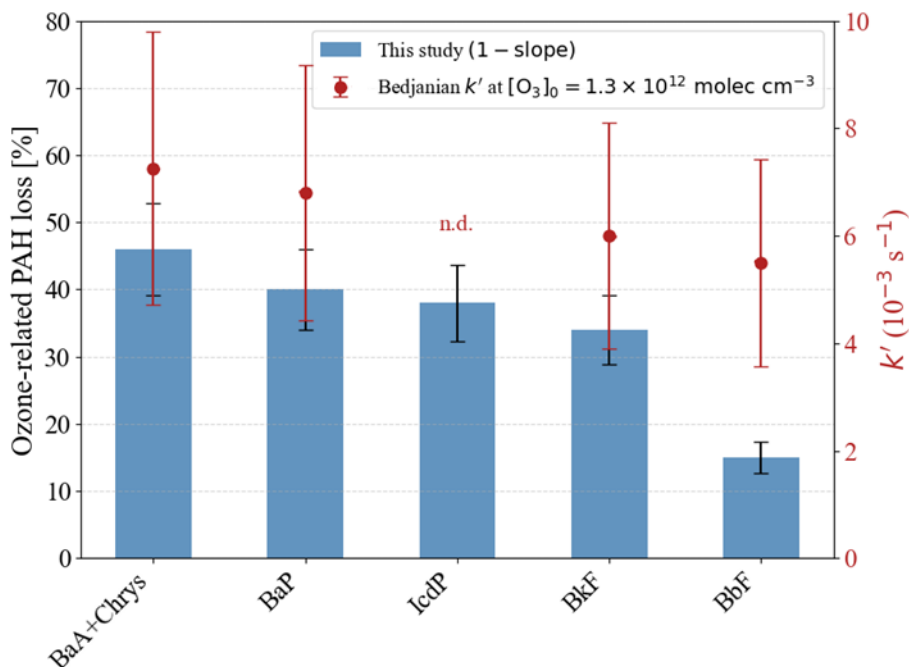


Figure 66 Compound-specific comparison of O_3 induced losses of particle-bound PAH. Blue bars (left axis) show the O_3 -attributable loss fraction from this study (1 – slope of the O_3 -contrast regression). Red symbols (right axis) show first-order consumption rate constants k' ($\times 10^{-3} \text{ s}^{-1}$) from Bedjanian & Nguyen (2010) for soot exposed to $[\text{O}_3]_0 = 1.3 \times 10^{12} \text{ molec cm}^{-3}$ at 290 K; red vertical whiskers indicate their reported variability. The red dashed lines simply connect compounds to guide the eye. “n.d.” = no k' reported (IcdP).

4. Conclusion

This study demonstrates the development and evaluation of a TSOD adapted for UFP sampling. Under controlled laboratory conditions, the TSOD removed O_3 effectively for O_3 mixing ratios of up to 200 ppbV and constant RH relative humidity of 53%. The same was observed during a five days field campaign, with varying ambient O_3 mixing ratios (0–65 ppbV) and RH relative humidity (38–99 %). No significant particle losses were observed in the 10–100 nm and 10–1000 nm range across various flow rates, with relative average deviation of 5%, remaining within instrumental uncertainty.

Utilizing a dual-channel approach, we compared the impact of upstream O_3 removal prior to filter based analysis of mass concentrations of selected UFP-bound marker compounds of diverse chemical properties and of well-known interest in atmospheric studies. O_3 -sensitive markers such as PAHs and 6PPD showed markable inter-channel differences: relative O_3 -induced losses reached 15–46 % for higher molecular weight PAHs and up to 48 % for 6PPD. In contrast, 6PPDq concentrations increased in the O_3 -exposed channel, consistent with in-situ formation from 6PPD. Quantitative comparison of absolute concentrations suggests a 6PPD to 6PPDq transformation of about 13 to 20 %, in agreement with previously reported

laboratory yields. BOAs showed no inter-channel effect, implying that the TSOD did not induce a measurable change in particle reactivity or phase distribution of these semi-volatile species. Such change would need to be large enough to overcome analytical variability, which we do not observe.

470 Without an upstream O₃ denuder, systematic sampling artefacts occur: PAHs and 6PPD are systematically and significantly underestimated, while oxidation products such as 6PPDq are overestimated due to in-situ ozonolysis. Thus, O₃ removal is a methodological requirement for quantitative chemical UFP analysis. The TSOD meets the requirements by (i) efficiently scrubbing O₃ at atmospherically relevant mixing ratios, (ii) introducing no measurable particle loss across sizes from 10 nm to 1000 nm, and (iii) not perturbing the gas–particle partitioning of semi-volatile BOAs.

475

Data Availability

Data will be made available upon request.

480

Acknowledgement

We thank the Bavarian Environment Agency (LfU) and the German Weather Service (DWD) for providing ozone and meteorological data.

485 This project is financed by the Bavarian State Ministry of the Environment and Consumer Protection. The article processing charges for this open-access publication were covered by the Forschungszentrum Jülich.

490

495

500

References

- Abdel-Shafy, H. I., & Mansour, M. S. M. (2016). A review on polycyclic aromatic hydrocarbons: Source, environmental impact, effect on human health and remediation. *Egyptian Journal of Petroleum*, 25(1), 107–123. <https://doi.org/10.1016/j.ejpe.2015.03.011>
- 505 Balducci, C., Cecinato, A., Paolini, V., Guerriero, E., Perilli, M., Romagnoli, P., Tortorella, C., Iacobellis, S., Giove, A., & Febo, A. (2018). Volatilization and oxidative artifacts of PM bound PAHs collected at low volume sampling (1): Laboratory and field evaluation. *Chemosphere*, 200, 106–115. <https://doi.org/10.1016/j.chemosphere.2018.02.090>
- Balmes, J. R., & Hansel, N. N. (2024). Tiny Particles, Big Health Impacts. *American Journal of Respiratory and Critical Care Medicine*, 210(11), 1291–1292. <https://doi.org/10.1164/rccm.202407-1476ED>
- 510 Bedjanian, Y., & Nguyen, M. L. (2010). Kinetics of the reactions of soot surface-bound polycyclic aromatic hydrocarbons with O₃. *Chemosphere*, 79(4), 387–393. <https://doi.org/10.1016/j.chemosphere.2010.02.009>
- Bell, M. L., Goldberg, R., Hogrefe, C., Kinney, P. L., Knowlton, K., Lynn, B., Rosenthal, J., Rosenzweig, C., & Patz, J. A. (2007). Climate change, ambient ozone, and health in 50 US cities. *Climatic Change*, 82(1–2), 61–76. <https://doi.org/10.1007/s10584-006-9166-7>
- 515 Cataldo, F. (2019). Protection Mechanism of Rubbers from Ozone Attack. *Ozone: Science & Engineering*, 41(4), 358–368. <https://doi.org/10.1080/01919512.2018.1542518>
- Christoffersen, T. S., Hjorth, J., Horie, O., Jensen, N. R., Kotzias, D., Molander, L. L., Neeb, P., Ruppert, L., Winterhalter, R., Virkkula, A., Wirtz, K., & Larsen, B. R. (1998). cis-pinic acid, a possible precursor for organic aerosol formation from ozonolysis of α -pinene. *Atmospheric Environment*, 32(10), 1657–1661. [https://doi.org/10.1016/S1352-2310\(97\)00448-](https://doi.org/10.1016/S1352-2310(97)00448-2)
- 520 2
- Cooper, O. R., Parrish, D. D., Ziemke, J., Balashov, N. V., Cupeiro, M., Galbally, I. E., Gilge, S., Horowitz, L., Jensen, N. R., Lamarque, J. F., Naik, V., Oltmans, S. J., Schwab, J., Shindell, D. T., Thompson, A. M., Thouret, V., Wang, Y., & Zbinden, R. M. (2014). Global distribution and trends of tropospheric ozone: An observation-based review. In *Elementa* (Vol. 2). BioOne. <https://doi.org/10.12952/journal.elementa.000029>
- 525 Delgado-Saborit, J. M., Stark, C., & Harrison, R. M. (2014). Use of a Versatile High Efficiency Multiparallel Denuder for the Sampling of PAHs in Ambient Air: Gas and Particle Phase Concentrations, Particle Size Distribution and Artifact Formation. *Environmental Science & Technology*, 48(1), 499–507. <https://doi.org/10.1021/es402937d>
- Denjean, C., Formenti, P., Picquet-Varrault, B., Camredon, M., Pangui, E., Zapf, P., Katrib, Y., Giorio, C., Tapparo, A., Temime-Roussel, B., Monod, A., Aumont, B., & Doussin, J. F. (2015). Aging of secondary organic aerosol generated from the ozonolysis of α -pinene: effects of ozone, light and temperature. *Atmospheric Chemistry and Physics*, 15(2), 883–897. <https://doi.org/10.5194/acp-15-883-2015>
- 530 Eckenberger, E., Mittereder, A., Gawlitta, N., Schnelle-Kreis, J., Sklorz, M., Brüggemann, D., Zimmermann, R., & Nölscher, A. C. (2025). Performance evaluation of four cascade impactors for airborne ultrafine-particle (UFP) collection: the

- influence of particle type, concentration, mass, and chemical nature. *Aerosol Research*, 3(1), 45–64.
535 <https://doi.org/10.5194/ar-3-45-2025>
- Emberson, L. (2020). Effects of ozone on agriculture, forests and grasslands. *Philosophical Transactions of the Royal Society A: Mathematical, Physical and Engineering Sciences*, 378(2183), 20190327. <https://doi.org/10.1098/rsta.2019.0327>
- Ernle, L., Ringsdorf, M. A., & Williams, J. (2023). Influence of ozone and humidity on PTR-MS and GC-MS VOC
540 measurements with and without a Na₂S₂O₃ ozone scrubber. *Atmospheric Measurement Techniques*, 16(5), 1179–
1194. <https://doi.org/10.5194/amt-16-1179-2023>
- European Committee for Standardization (CEN). (2008). *EN 15549:2008 – Air quality — Standard method for the
measurement of the concentration of benzo[a]pyrene and other polycyclic aromatic hydrocarbons in ambient air.*
- Fick, J., Pommer, L., Andersson, B., & Nilsson, C. (2001). Ozone Removal in the Sampling of Parts per Billion Levels of
Terpenoid Compounds: An Evaluation of Different Scrubber Materials. *Environmental Science & Technology*, 35(7),
545 1458–1462. <https://doi.org/10.1021/es0001456>
- Gaudel, A., Cooper, O. R., Ancellet, G., Barret, B., Boynard, A., Burrows, J. P., Clerbaux, C., Coheur, P.-F., Cuesta, J., Cuevas,
E., Doniki, S., Dufour, G., Ebojje, F., Foret, G., Garcia, O., Granados-Muñoz, M. J., Hannigan, J. W., Hase, F., Hassler,
B., ... Ziemke, J. (2018). Tropospheric Ozone Assessment Report: Present-day distribution and trends of tropospheric
ozone relevant to climate and global atmospheric chemistry model evaluation. *Elementa: Science of the Anthropocene*,
550 6. <https://doi.org/10.1525/elementa.291>
- Haddad, P., Jeong, H., Kappeler, R., Altug, H., Andersen, Z. J., Bergmann, M., Boogaard, H., Kutlar, M. J., Lim, Y. H., Loft,
S., Pohl, T., & Hoffmann, B. (2024). Systematic review on health effects of long-term exposure to UFP. *ISEE Conference
Abstracts*, 2024(1). <https://doi.org/10.1289/isee.2024.0574>
- Ho, S. S. H., Ip, H. S. S., Ho, K. F., Dai, W.-T., Cao, J., & Ng, L. P. T. (2013). Technical Note: Concerns on the Use of Ozone
555 Scrubbers for Gaseous Carbonyl Measurement by DNPH-Coated Silica Gel Cartridge. *Aerosol and Air Quality
Research*, 13(4), 1151–1160. <https://doi.org/10.4209/aaqr.2012.11.0313>
- Hu, X., Zhao, H. N., Tian, Z., Peter, K. T., Dodd, M. C., & Kolodziej, E. P. (2022). Transformation Product Formation upon
Heterogeneous Ozonation of the Tire Rubber Antioxidant 6PPD (*N* -(1,3-dimethylbutyl)- *N* '-phenyl- *p* -
phenylenediamine). *Environmental Science & Technology Letters*, 9(5), 413–419.
560 <https://doi.org/10.1021/acs.estlett.2c00187>
- Ji, Z., Zhang, N., Huang, C., Duan, X., Ren, D., & Huo, Z. (2024). The Degradation of Polycyclic Aromatic Hydrocarbons
(PAHs) by Ozone-Based Advanced Oxidation Processes: A Review. *Ozone: Science & Engineering*, 46(1), 26–42.
<https://doi.org/10.1080/01919512.2023.2192751>
- Kristensen, K., Bilde, M., Aalto, P. P., Petäjä, T., & Glasius, M. (2016). Denuder/filter sampling of organic acids and
565 organosulfates at urban and boreal forest sites: Gas/particle distribution and possible sampling artifacts. *Atmospheric
Environment*, 130, 36–53. <https://doi.org/10.1016/j.atmosenv.2015.10.046>

- Kristensen, K., Watne, Å. K., Hammes, J., Lutz, A., Petäjä, T., Hallquist, M., Bilde, M., & Glasius, M. (2016). High-Molecular Weight Dimer Esters Are Major Products in Aerosols from α -Pinene Ozonolysis and the Boreal Forest. *Environmental Science & Technology Letters*, 3(8), 280–285. <https://doi.org/10.1021/acs.estlett.6b00152>
- 570 Kuwabara, H., Sekiguchi, K., Sankoda, K., Sakurai, K., Yamaguchi, R., Furuuchi, M., & Hata, M. (2016). Evaluation of Artifacts Generated during Collection of Ultrafine Particles Using an Inertial Filter Sampler. *Aerosol and Air Quality Research*, 16(12), 3063–3074. <https://doi.org/10.4209/aaqr.2015.12.0679>
- Kwamena, N.-O. A., Clarke, J. P., Kahan, T. F., Diamond, M. L., & Donaldson, D. J. (2007). Assessing the importance of heterogeneous reactions of polycyclic aromatic hydrocarbons in the urban atmosphere using the Multimedia Urban
- 575 Model. *Atmospheric Environment*, 41(1), 37–50. <https://doi.org/10.1016/j.atmosenv.2006.08.016>
- Kwon, H.-S., Ryu, M. H., & Carlsten, C. (2020). Ultrafine particles: unique physicochemical properties relevant to health and disease. *Experimental & Molecular Medicine*, 52(3), 318–328. <https://doi.org/10.1038/s12276-020-0405-1>
- Li, Q.-Q., Guo, Y.-T., Yang, J.-Y., & Liang, C.-S. (2023). Review on main sources and impacts of urban ultrafine particles: Traffic emissions, nucleation, and climate modulation. *Atmospheric Environment: X*, 19, 100221.
- 580 <https://doi.org/10.1016/j.aeaoa.2023.100221>
- Liffick, G. L. (1970). *An Investigation of the Removal of Ozone by Activated Charcoal*. Oregon State University.
- Liu, K., Duan, F., He, K., Ma, Y., & Cheng, Y. (2014). Investigation on sampling artifacts of particle associated PAHs using ozone denuder systems. *Frontiers of Environmental Science & Engineering*, 8(2), 284–292. <https://doi.org/10.1007/s11783-013-0555-7>
- 585 Liu, Y., Sklorz, M., Schnelle-Kreis, J., Orasche, J., Ferge, T., Kettrup, A., & Zimmermann, R. (2006). Oxidant denuder sampling for analysis of polycyclic aromatic hydrocarbons and their oxygenated derivatives in ambient aerosol: Evaluation of sampling artefact. *Chemosphere*, 62(11), 1889–1898. <https://doi.org/10.1016/j.chemosphere.2005.07.049>
- Marval, J., & Tronville, P. (2022). Ultrafine particles: A review about their health effects, presence, generation, and measurement in indoor environments. *Building and Environment*, 216, 108992. <https://doi.org/10.1016/j.buildenv.2022.108992>
- 590 Monks, P. S., Archibald, A. T., Colette, A., Cooper, O., Coyle, M., Derwent, R., Fowler, D., Granier, C., Law, K. S., Mills, G. E., Stevenson, D. S., Tarasova, O., Thouret, V., von Schneidemesser, E., Sommariva, R., Wild, O., & Williams, M. L. (2015). Tropospheric ozone and its precursors from the urban to the global scale from air quality to short-lived climate forcer. *Atmospheric Chemistry and Physics*, 15(15), 8889–8973. <https://doi.org/10.5194/acp-15-8889-2015>
- 595 Mutzel, A., Rodigast, M., Iinuma, Y., Böge, O., & Herrmann, H. (2016). Monoterpene SOA – Contribution of first-generation oxidation products to formation and chemical composition. *Atmospheric Environment*, 130, 136–144. <https://doi.org/10.1016/j.atmosenv.2015.10.080>
- Nikolaou, N., Bouwer, L. M., Dallavalle, M., Valizadeh, M., Stafoggia, M., Peters, A., Wolf, K., & Schneider, A. (2023). Improved daily estimates of relative humidity at high resolution across Germany: A random forest approach.
- 600 *Environmental Research*, 238, 117173. <https://doi.org/10.1016/j.envres.2023.117173>

- Oberdörster, G., Ferin, J., Gelein, R., Soderholm, S. C., & Finkelstein, J. (1992). Role of the alveolar macrophage in lung injury: studies with ultrafine particles. *Environmental Health Perspectives*, *97*, 193–199. <https://doi.org/10.1289/ehp.97-1519541>
- 605 Ofner, J., Krüger, H. U., Grothe, H., Schmitt-Kopplin, P., Whitmore, K., & Zetzsch, C. (2011). Physico-chemical characterization of SOA derived from catechol and guaiacol - A model substance for the aromatic fraction of atmospheric HULIS. *Atmospheric Chemistry and Physics*, *11*(1), 1–15. <https://doi.org/10.5194/acp-11-1-2011>
- Pöschl, U., Letzel, T., Schauer, C., & Niessner, R. (2001). Interaction of Ozone and Water Vapor with Spark Discharge Soot Aerosol Particles Coated with Benzo[*a*]pyrene: O₃ and H₂O Adsorption, Benzo[*a*]pyrene Degradation, and Atmospheric Implications. *The Journal of Physical Chemistry A*, *105*(16), 4029–4041. <https://doi.org/10.1021/jp004137n>
- 610 Prather, M. J., & Zhu, X. (2024). Lifetimes and timescales of tropospheric ozone. *Elem Sci Anth*, *12*(1). <https://doi.org/10.1525/elementa.2023.00112>
- RAVINDRA, K., SOKHI, R., & VANGRIEKEN, R. (2008). Atmospheric polycyclic aromatic hydrocarbons: Source attribution, emission factors and regulation. *Atmospheric Environment*, *42*(13), 2895–2921. <https://doi.org/10.1016/j.atmosenv.2007.12.010>
- 615 Rossomme, E., Hart-Cooper, W. M., Orts, W. J., McMahan, C. M., & Head-Gordon, M. (2023). Computational Studies of Rubber Ozonation Explain the Effectiveness of 6PPD as an Antidegradant and the Mechanism of Its Quinone Formation. *Environmental Science & Technology*, *57*(13), 5216–5230. <https://doi.org/10.1021/acs.est.2c08717>
- Schraufnagel, D. E. (2020). The health effects of ultrafine particles. *Experimental & Molecular Medicine*, *52*(3), 311–317. <https://doi.org/10.1038/s12276-020-0403-3>
- 620 Shiraiwa, M., Ammann, M., Koop, T., & Pöschl, U. (2011). Gas uptake and chemical aging of semisolid organic aerosol particles. *Proceedings of the National Academy of Sciences*, *108*(27), 11003–11008. <https://doi.org/10.1073/pnas.1103045108>
- Subramanian, R., Khlystov, A. Y., Cabada, J. C., & Robinson, A. L. (2004). Positive and Negative Artifacts in Particulate Organic Carbon Measurements with Denuded and Undenuded Sampler Configurations Special Issue of *Aerosol Science and Technology* on Findings from the Fine Particulate Matter Supersites Program. *Aerosol Science and Technology*, *38*(sup1), 27–48. <https://doi.org/10.1080/02786820390229354>
- 625 Takizawa, M., Okuwaki, A., & Okabe, T. (1973). The Chemical Behavior of Low Valence Sulfur Compounds. VIII. The Oxidation of Sodium Thiosulfate with Ozone. *Bulletin of the Chemical Society of Japan*, *46*(12), 3785–3789. <https://doi.org/10.1246/bcsj.46.3785>
- 630 WHO global air quality guidelines. Particulate matter (PM_{2.5} and PM₁₀), ozone, nitrogen dioxide, sulfur dioxide and carbon monoxide. (n.d.).
- Williams, E. L., & Grosjean, D. (1990). Removal of atmospheric oxidants with annular denuders. *Environmental Science & Technology*, *24*(6), 811–814.

- 635 YataVELLI, R. L. N., Lopez-Hilfiker, F., Wargo, J. D., Kimmel, J. R., Cubison, M. J., Bertram, T. H., Jimenez, J. L., Gonin, M., Worsnop, D. R., & Thornton, J. A. (2012). A Chemical Ionization High-Resolution Time-of-Flight Mass Spectrometer Coupled to a Micro Orifice Volatilization Impactor (MOVI-HRToF-CIMS) for Analysis of Gas and Particle-Phase Organic Species. *Aerosol Science and Technology*, *46*(12), 1313–1327. <https://doi.org/10.1080/02786826.2012.712236>
- 640 YataVELLI, R. L. N., Stark, H., Thompson, S. L., Kimmel, J. R., Cubison, M. J., Day, D. A., Campuzano-Jost, P., Palm, B. B., Hodzic, A., Thornton, J. A., Jayne, J. T., Worsnop, D. R., & Jimenez, J. L. (2014). Semicontinuous measurements of gas–particle partitioning of organic acids in a ponderosa pine forest using a MOVI-HRToF-CIMS. *Atmospheric Chemistry and Physics*, *14*(3), 1527–1546. <https://doi.org/10.5194/acp-14-1527-2014>
- 645 Young, P. J., Archibald, A. T., Bowman, K. W., Lamarque, J.-F., Naik, V., Stevenson, D. S., Tilmes, S., Voulgarakis, A., Wild, O., Bergmann, D., Cameron-Smith, P., Cionni, I., Collins, W. J., Dalsøren, S. B., Doherty, R. M., Eyring, V., Faluvegi, G., Horowitz, L. W., Josse, B., ... Zeng, G. (2013). Pre-industrial to end 21st century projections of tropospheric ozone from the Atmospheric Chemistry and Climate Model Intercomparison Project (ACCMIP). *Atmospheric Chemistry and Physics*, *13*(4), 2063–2090. <https://doi.org/10.5194/acp-13-2063-2013>
- 650 Yu, J., Griffin, R. J., Cocker, D. R., Flagan, R. C., Seinfeld, J. H., & Blanchard, P. (1999). Observation of gaseous and particulate products of monoterpene oxidation in forest atmospheres. *Geophysical Research Letters*, *26*(8), 1145–1148. <https://doi.org/10.1029/1999GL900169>
- Zhang, J. (Jim), Wei, Y., & Fang, Z. (2019). Ozone Pollution: A Major Health Hazard Worldwide. *Frontiers in Immunology*, *10*. <https://doi.org/10.3389/fimmu.2019.02518>
- 655 Zhao, H. N., Hu, X., Tian, Z., Gonzalez, M., Rideout, C. A., Peter, K. T., Dodd, M. C., & Kolodziej, E. P. (2023). Transformation Products of Tire Rubber Antioxidant 6PPD in Heterogeneous Gas-Phase Ozonation: Identification and Environmental Occurrence. *Environmental Science & Technology*, *57*(14), 5621–5632. <https://doi.org/10.1021/acs.est.2c08690>
- Zhao, Z., Hao, J., LI, J., & WU, S. (2008). Second organic aerosol formation from the ozonolysis of α -pinene in the presence of dry submicron ammonium sulfate aerosol. *Journal of Environmental Sciences*, *20*(10), 1183–1188. [https://doi.org/10.1016/S1001-0742\(08\)62207-X](https://doi.org/10.1016/S1001-0742(08)62207-X)
- 660 Zhou, S., Hwang, B. C. H., Lakey, P. S. J., Zuend, A., Abbatt, J. P. D., & Shiraiwa, M. (2019). Multiphase reactivity of polycyclic aromatic hydrocarbons is driven by phase separation and diffusion limitations. *Proceedings of the National Academy of Sciences*, *116*(24), 11658–11663. <https://doi.org/10.1073/pnas.1902517116>

Supplementary Information

670

Sodium Thiosulfate-Coated Ceramic Denuders for Ozone Removal in Ultrafine Particle Sampling: Performance from Laboratory to Field

675 Elisabeth Eckenberger¹, Andreas Mittereder², Nadine Gawlitta^{3,4}, Martin Sklorz^{3,4}, Dieter Brüggemann²,
Ralf Zimmermann^{3,4}, Anke C Nölscher^{1*}

¹ Bayreuth Center of Ecology and Environmental Research (BayCEER), University of Bayreuth, Germany

² Department of Engineering Thermodynamics and Transport Processes, University of Bayreuth, Bayreuth, Germany

680 ³ Joint Mass Spectrometry Centre (JMSC) at Comprehensive Molecular Analytics, Helmholtz Zentrum München, Neuherberg,
Germany

⁴ JMSC at Chair of Analytical Chemistry, Institute of Chemistry, University of Rostock, Rostock, Germany

* now at: Institute of Climate and Energy Systems, ICE-3: Troposphere, Forschungszentrum Jülich GmbH, Jülich, Germany,
and Institute of Geophysics and Meteorology, University of Cologne, Cologne, Germany

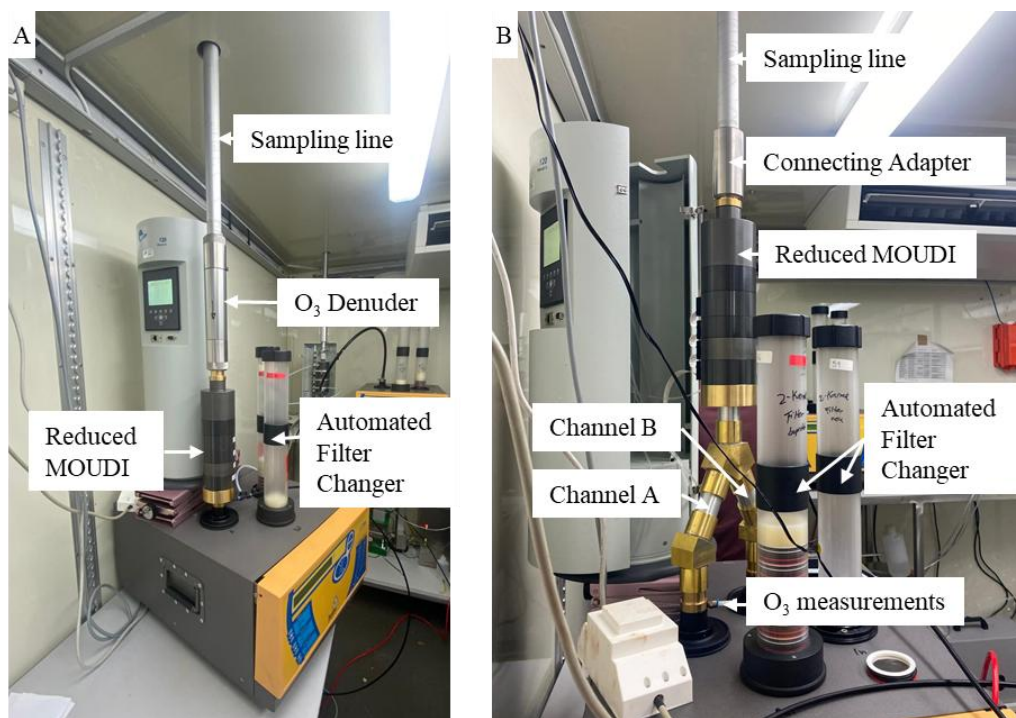
685 *Correspondence to:* Elisabeth Eckenberger (Elisabeth.eckenberger@uni-bayreuth.de), Anke C. Nölscher (a.noelscher@fz-
juelich.de)

690



695

Figure S1 Photograph of the ceramic honeycomb body ($\text{\O} 25,4 \times 50\text{mm}$) used as substrate for Na_2SO_3 coating in this study.



700

Figure S2 A Picture of one sampling setup, where the TSOD are in a stainless steel housing which is connected above the reduced MOUDI impactor. Such a housing is also used to connect the TSOD from the BATCH to the measurement devices as described in sections 2.2 and 2.3. B Picture of the sampling setup described in section 2.4. The uncoated or coated denuders (depending on the experiment) are behind the MOUDI impactor in channels A and B, directly placed above the UFP filter which was used for analysis.

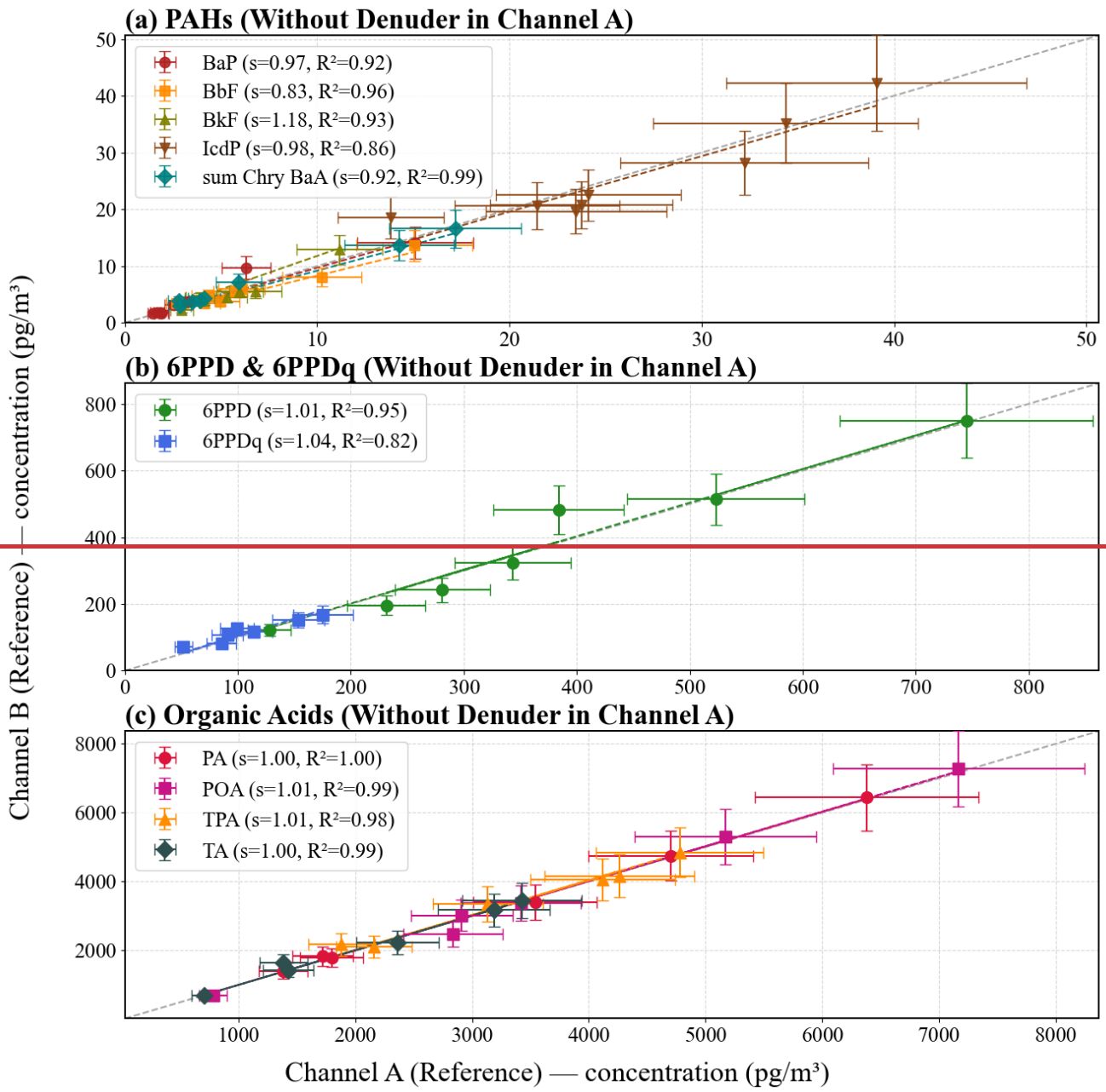
705

Table S1: Specifications regarding the different marker compounds that were analyzed and chosen for this study.

Parameter	HPLC-MS neg	HPLC-MS pos	HPLC-FLD
Analytical column	Gemini 5u C18 110A (150 mm x 4.6 mm, 5 μm)	Gemini 5u C18 110A (150 mm x 4.6 mm, 5 μm)	EC 125/4 Nucleosil 100-5 C18 HD (125 mm x 4 mm, 5 μm)
Column temperature	40 °C	30 °C	30 °C
Injection volume	20 μL	20 μL	25 μL
Autosampler temperature	–	–	-5 °C
Flow rate	0.5 mL/min	0.3 - 0.5 mL/min	1 mL/min
Gradient	A) 80% ACN, B) 4 mM HCOOH 0 min 5% A 1 min 5% A 18 min 50% A 21 min 100% A 29 min 100% A 31 min 5% A	A) 80%MeOH, B) 4 mM HCOOH 0 min 50% A 3 min 80% A 12 min 100% A 18 min 90% A 20 min 50% A 25 min 75% A	A) ACN, B) H₂O (Milli-pore) 0 min 60% A 5 min 70% A 8 min 70% A 12 min 80% A 15 min 80% A 19 min 90% A 22 min 60% A
Detector	MSD Time ESI(-)-m/z-ions 0 min 207 8 min 111, 157, 171, 185 18 min 121, 135, 183 25 min 193, 217	MSD Time ESI(+)-m/z-ions 0 min 212, 227, 269 12 min 257, 261, 299	FLD Time λ_{ex} / λ_{em} [nm] 0 min 259 / 386 3.3 min 242 / 388 5.8 min 250 / 370 7.5 min 270 / 390 13 min 290 / 430

Table S2: Specifications regarding the different marker compounds that were analyzed and chosen for this study.

Marker	Method	Recovery	LOD _{Air}	External standard calculation	
			[pg/m ³] 21.6 m ³	Response factor [AU/μg/L]	R ²
POA	HPLC-MS neg	101±6%	268.06	1833	0.98
PA	HPLC-MS neg	84±6%	373.14	4415	0.99
TA	HPLC-MS neg	85±6%,	268.06	3352	0.99
TPA	HPLC-MS neg	96±6%,	343.52	2781	0.99
6PPD	HPLC-MS pos	75±7%	20.09	26766	0.98
6PPDq	HPLC-MS pos	81±7%	24.54	21767	0.99
BaP	HPLC-FLD/UV	78±5%	3.245	10.12	1.00
BbF	HPLC-FLD/UV	74±4%	4.025	12.15	1.00
IcdP	HPLC-FLD/UV	70±4%	3.052	3.29	1.00
Sum Chry BaA	HPLC-FLD/UV	97±5%	2.855	9.68	1.00
BkF	HPLC-FLD/UV	89±6%	2.679	11.80	1.00



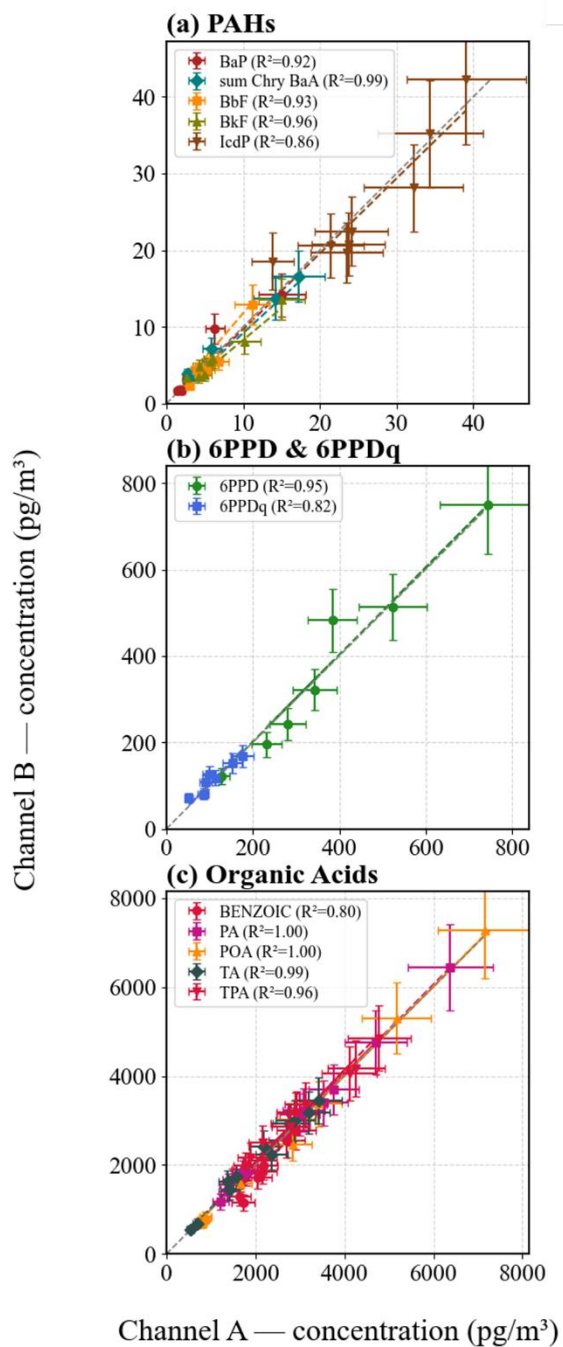


Figure S33 Comparison of PAH concentrations between Channel A and Channel B without the deployment of the TSOD. Regression slopes (s) and coefficients of determination (R^2) indicate high inter-channel agreement in the absence of O_3 removal.